

1 **Elevational Dependence of Global Forest Fires and Associated Aerosol Optical**
2 **Depth: Drivers and Decoupling**

3 Qiaomin Pei ¹, Chuanfeng Zhao ^{1,2*}, Xing Yan ^{3,4}, Xingchuan Yang ⁵, Annan Chen ¹, Xin Wan ⁶

4 *1 Department of Atmospheric and Oceanic Sciences, School of Physics, Peking University, Beijing*
5 *100871, China.*

6 *2 Institute of Carbon Neutrality, Peking University, Beijing 100871, China.*

7 *3 State Key Laboratory of Earth Surface Processes and Disaster Risk Reduction, Faculty of*
8 *Geographical Science, Beijing Normal University, Beijing 100875, China*

9 *4 Advanced Interdisciplinary Institute of Satellite Applications, Faculty of Geographical*
10 *Science, Beijing Normal University, Beijing 100875, China*

11 *5 College of Resource Environment and Tourism, Capital Normal University, Beijing 100048, China*

12 *6 State Key Laboratory of Tibetan Plateau Earth System, Resources and Environment (TPESRE),*
13 *Institute of Tibetan Plateau Research, Chinese Academy of Sciences, Beijing 100101, China*

14

15 Correspondence to: Chuanfeng Zhao (cfzhao@pku.edu.cn)

16

17 **Abstract**

18 Forest fires have become an escalating environmental and ecological issue
19 worldwide over the past decades. However, a knowledge gap persists in globally
20 assessing how topography modulates wildfire behavior. Here we quantify global
21 spatiotemporal patterns of forest fire activity and associated aerosol optical depth
22 (AOD), together with elevation-dependent controls, using satellite observations from
23 2012 to 2024. The analysis reveals a slight yet significant increase in fire occurrence,
24 accompanied by a strong positive association with fine-mode AOD (FAOD). In contrast,
25 coarse-mode AOD (CAOD) shows little response, implying that wildfire emissions
26 mainly contribute to the fine aerosol fraction. Forest fire occurrence declines
27 systematically with elevation, with most fires concentrated below 600 m. In contrast,
28 FAOD exhibits elevated mean values and increasing trends at mid-elevations (600–
29 1400 m), revealing a decoupling between fire frequency and aerosol loading. This
30 divergence is consistent with shifts in forest-type composition and topographically
31 modulated smoke transport, including aerosol self-lifting driven by radiative absorption
32 and atmospheric convection. Elevation-stratified multiple linear regression analyses
33 incorporating the Fire Weather Index, leaf area index, temperature, wind speed, and
34 precipitation indicate that fire activity is primarily governed by fuel availability and
35 aridity. Precipitation exerts a consistent suppressive effect across elevations, while wind
36 speed enhances fuel drying and fire spread at mid-elevations. Overall, these results
37 identify elevation as a key organizing factor linking forest fires, aerosol emissions, and
38 their underlying drivers, providing new constraints for wildfire risk assessment and
39 fire–aerosol interactions under a changing climate.

40

411. **Introduction**

42 Wildfires represent a key component of the Earth system, influencing ecosystems,
43 atmospheric composition, carbon cycling, climate, and public health on a global scale
44 (Bowman et al., 2009; Andela et al., 2017; Qian, 2025; Yang et al., 2022; Yang et al.,
45 2021a). Over the past decade, the societal and environmental consequences of wildfires
46 have attracted increasing scientific and public attention (Abatzoglou et al., 2025).
47 Concurrently, ongoing climate warming has intensified fire-conducive weather,
48 increasing the probability of wildfire occurrence, particularly large and extreme events
49 (Jones et al., 2024; Abatzoglou et al., 2025). Elevated temperatures and prolonged
50 dryness further reduce fuel moisture, raising fire susceptibility in biomass-rich forests
51 (Jones et al., 2024; Jolly et al., 2015).

52 Forests constitute the most extensive terrestrial biome and serve as a major
53 component of the global carbon budget (Pan et al., 2011). Despite their critical role,
54 these ecosystems are becoming increasingly vulnerable to wildfire disturbances
55 (Keywood et al., 2013). While the total burned area worldwide has shown a declining
56 tendency in recent decades, fire occurring in forested regions have become more
57 frequent and more severe, with average fire size, duration, and intensity increasing by
58 two- to threefold over recent decades (Zheng et al., 2021; Cunningham et al., 2024;
59 Parisien et al., 2023; Canadell et al., 2021). Escalating occurrences of extreme fires
60 threaten forest stability and recovery capacity, potentially undermining essential
61 ecosystem functions and services, including long-term carbon storage (Ward et al.,
62 2020; Gatti et al., 2021). In contrast to grasslands, forest fires release greater amounts
63 of carbon dioxide per unit area, and the reestablishment of carbon sinks after burning
64 is generally slow, which may generate a positive climate-fire feedback (Zheng et al.,
65 2021). These risks are further intensified by climate change, which promotes fuel aridity,
66 extreme fire weather, and longer fire seasons, thereby increasing the probability of
67 large-scale biomass burning (Kirchmeier-Young et al., 2024; Wang et al., 2025). Large
68 and extreme fires are also promoted by human disturbance and land-use change,
69 particularly in tropical forests where frequent human ignitions and ongoing forest

70 degradation strongly drive fire activity (Lapola et al., 2023; Yang et al., 2023). By
71 completely or partially removing aboveground vegetation, wildfires fundamentally
72 alter forest structure and function (Kim et al., 2025), making forest fire activity an
73 increasingly urgent global environmental and ecological concern.

74 The combustion of biomass in forest fires releases significant quantities of
75 aerosols and trace gases into the atmosphere, leading to pronounced air quality
76 deterioration not only near source regions but also in distant areas affected by long-
77 range smoke transport (Ma et al., 2025; Zhang et al., 2025; Fan et al., 2021; Xu et al.,
78 2025). Smoke-related pollution markedly increases annual mean PM_{2.5} exposure,
79 contributing to thousands of premature deaths and billions of U.S. dollars in economic
80 losses each year (Ma et al., 2025; Zhang et al., 2025). In addition to these air quality
81 impacts, smoke aerosols influence the Earth's radiation balance and climate system
82 through both direct interactions with solar radiation (scattering and absorption) and
83 indirect effects associated with cloud microphysics (Keywood et al., 2013; Andreae et
84 al., 2004; Blanchard-Wrigglesworth et al., 2025). Wildfire emissions induce contrasting
85 thermal effects, characterized by surface cooling and atmospheric warming, which
86 modify atmospheric stability, vertical transport, circulation patterns, and regional
87 hydrology, ultimately driving significant climatic responses (Menon et al., 2002; Koren
88 et al., 2004; Lau et al., 2006; Blanchard-Wrigglesworth et al., 2025; Pei et al., 2025).
89 Moreover, wildfire-derived aerosols affect atmospheric and oceanic biogeochemistry
90 by modulating nutrient deposition and photosynthetic activity in marine ecosystems
91 (Hamilton et al., 2022; Tang et al., 2021). Consequently, wildfire emissions exert broad
92 effects on air quality, the global radiation balance, and coupled climate–biogeochemical
93 systems.

94 Substantial studies have elucidated that vegetation cover, fire weather, climate and
95 topography jointly govern the probability and severity of forest fires (Parks et al., 2018;
96 Birch et al., 2015; Whitman et al., 2018; Wang et al., 2022c; Yu et al., 2020). Besides
97 fire weather and climate forcing, vegetation characteristics and topographic controls are
98 critical determinants of fire severity, particularly in mountainous terrain (Birch et al.,

99 2015; Walker et al., 2020). Live fuel availability, represented by vegetation cover, has
100 been shown to strongly regulate wildfire severity. Analyses of 19 forested ecoregions
101 across the western United States for 2002–2015 highlighted it as the dominant control
102 (Parks et al., 2018), with comparable relationships documented in both the northern
103 Rocky Mountains (Birch et al., 2015) and North American boreal forests (Walker et al.,
104 2020; Whitman et al., 2018). Using a machine-learning approach, Jones et al. (2024)
105 categorized global forest ecoregions into 12 pyromes and showed that increases in
106 forest cover and ecosystem productivity substantially enhanced wildfire emissions.
107 Topographic factors—such as elevation, aspect, and slope—have also been shown to
108 exert substantial influence on burn severity across diverse regions, including China and
109 Canada (Huang et al., 2020; Whitman et al., 2018). Notably, investigations from the
110 Canadian Rocky Mountains reported strong associations between elevation and fire
111 activity (Rogean and Armstrong, 2017). Despite these advances, global-scale
112 assessments of the relationship between topography and fire regimes remain limited
113 relative to the extensive focus on vegetation-related drivers. This gap is notable given
114 that topography can substantially enhance fire spread and promote erratic fire behavior
115 (Sharples et al., 2012).

116 This work examines the influence of topography on global forest fire activity
117 through a comprehensive analysis of spatial fire patterns. Building on evidence from
118 Canadian forests identifying elevation as a key topographic control (Wang et al., 2025),
119 we focus on elevation as a central organizing factor. This study focuses on three main
120 objectives: (i) describing the global spatial distribution of fire pixel counts and their
121 associations with aerosol optical depth (AOD) over forested regions; (ii) assessing the
122 extent to which elevation shapes the spatial patterns of both fires and AOD; and (iii)
123 determining the key factors that control the elevation–fire relationship. To interpret
124 these patterns, multiple explanatory variables, including fuel load, forest type, and fire
125 weather, are jointly analyzed. By elucidating elevation-dependent fire dynamics, this
126 work provides a scientific basis for adaptive fire management, elevation-informed fuel
127 treatments, post-fire hazard mitigation, and ecologically informed fire use to support

128 biodiversity conservation in the face of persistent climate warming.

129 **2. Materials and methods**

130 **2.1 Satellite-based wildfire observations**

131 We utilized active fire observations from the Visible Infrared Imaging Radiometer
132 Suite (VIIRS) sensors carried by the Suomi NPP and NOAA-20 platforms. These
133 measurements capture combustion-related thermal signals at approximately 375 m
134 resolution. To facilitate large-scale analysis, individual fire detections were spatially
135 aggregated onto a $0.1^\circ \times 0.1^\circ$ global grid, and the number of detections within each cell
136 was used as a metric of fire occurrence. Daily wildfire activity was characterized using
137 the combined daytime and nighttime VIIRS observations, accounting for both fire
138 occurrence and intensity. Fire detections were spatially overlaid with a forest land-cover
139 mask to extract events occurring within forested pixels, and only grid cells with more
140 than one active fire detection during 2012–2024 were retained to ensure data robustness.
141 To enhance data reliability, fire pixels flagged as “low confidence” (confidence level
142 ‘1’) were excluded from the analysis.

143 **2.2 Vegetation types, elevation, and fire weather data**

144 Land cover information was characterized by using the MODIS land cover type
145 dataset at 500 m resolution, available through NASA’s Land Processes Distributed
146 Active Archive Center (LP DAAC). Topographic characteristics were represented using
147 the General Bathymetric Chart of the Oceans (GEBCO) 2024 gridded data, which
148 provides global elevation and bathymetry data at 15-arc-second resolution (~500 m)
149 (Harper and Sandwell, 2024). To ensure spatial consistency, land cover and elevation
150 datasets were resampled to match the analysis grid. Forest categories and elevation
151 values at fire locations were then extracted using nearest-neighbor interpolation.
152 Forested regions were grouped into five major types: evergreen needleleaf (ENF),
153 evergreen broadleaf (EBF), deciduous needleleaf (DNF), deciduous broadleaf (DBF),
154 and mixed forest (MF). Elevation was stratified into 20 zones using 100 m intervals
155 below 2000 m. Given the relatively low number of fire detections at higher elevations,
156 all regions above 2000 m were combined into a single category to ensure sufficient

157 sample sizes and enhance the robustness of subsequent trend analyses.

158 We employed the Canadian Forest Fire Weather Index (FWI) system to
159 characterize weather conditions that favor wildfire development and to assess climate-
160 driven variability in fire danger (Su et al., 2025; Liu et al., 2023; Van Wagner, 1987).
161 The index is calculated from standard meteorological inputs, including near-surface air
162 temperature, wind speed, relative humidity, and accumulated total precipitation over
163 the preceding 24-hour (Van Wagner, 1987). Daily FWI data with a resolution of 0.25°
164 $\times 0.25^\circ$ from 2012 to 2024 are obtained from the historical fire danger index archives.
165 Supplementary meteorological parameters, such as 2 m air temperature (2mT), 10 m
166 wind speed (10mW), and the max daily total precipitation, were extracted from the
167 ERA5 reanalysis produced by the European Centre for Medium-Range Weather
168 Forecasts (ECMWF). Monthly means of FWI and meteorological variables were
169 calculated for subsequent analyses with forest fire activity.

170 **2.3 Satellite-based FAOD and CAOD retrievals**

171 Size-resolved aerosol optical depths at 500 nm, including the fine (FAOD) and
172 coarse (CAOD) fractions, were estimated using SIDN (Simultaneous FAOD–CAOD
173 Inversion Deep Neural Network) algorithm. The inversion is physically constrained by
174 incorporating interactions between the two aerosol size classes, thereby enhancing
175 retrieval reliability (Luo et al., 2024; Chen et al., 2025). SIDN integrates multi-source
176 satellite observations with meteorological reanalysis data and is trained against high-
177 quality AERONET measurements using a shared representation learning strategy based
178 on the EntityDenseNet architecture. By dynamically balancing FAOD and CAOD
179 contributions during training, SIDN improves retrieval accuracy and internal
180 consistency across diverse aerosol regimes. A comprehensive description of the model
181 architecture, training procedure, and validation is provided in the above references and
182 is not repeated here. Extensive evaluations against independent ground-based
183 observations demonstrate that SIDN outperforms conventional satellite products,
184 yielding reduced uncertainties and improved spatial completeness, particularly under
185 cloudy and complex surface conditions. In addition, the deep-learning framework

186 trained with AERONET observations substantially improves retrieval accuracy and
187 stability across different aerosol regimes, making the dataset particularly suitable for
188 investigating wildfire–aerosol interactions on a global scale. The resulting daily global
189 FAOD and CAOD dataset spans 2012–2024 at a spatial resolution of 0.5°. Because the
190 spatial resolution of the AOD data is coarser than that of the forest fire dataset, a nearest-
191 neighbor approach was used to match the datasets. This method preserves the original
192 aerosol observations without introducing artificial smoothing or interpolation effects
193 and has been widely applied in satellite data matching studies. Although the spatial
194 resolution mismatch may introduce some uncertainties, its impact is expected to be
195 limited for the large-scale analyses conducted in this study.

196 **2.4 Temporal trends analysis**

197 Temporal trends in wildfire activity were assessed using linear regression applied
198 to annual fire pixel counts aggregated at 0.1° × 0.1° resolution. For each grid cell, a
199 linear regression was fitted between the natural logarithm of annual fire pixel counts
200 and time, with statistical significance determined at $p < 0.05$. The regression slope was
201 exponentiated to estimate the annual percentage change in fire occurrence. For the
202 global and forest-type–specific assessments, annual records were further processed
203 with a 3-year centered moving average, which filters out short-term interannual noise.
204 To verify the stability of the detected trends, we employed the Mann–Kendall non-
205 parametric test in combination with the Theil–Sen estimator, which provide outlier-
206 insensitive assessments of trend direction and magnitude. The Theil–Sen slope was then
207 derived for grid cells showing significant changes, expressed as

$$208 \quad SFC = \text{median} \left(\frac{FC_j - FC_i}{j - i} \right), 2012 \leq i < j \leq 2024$$

209 where SFC denotes the median rate of change, and FC_i and FC_j represent fire pixel
210 counts at moments i and j , respectively.

211 Trends in AOD over 2012–2024 were analyzed using the same logarithmic linear
212 regression framework to ensure comparability with fire pixel count trends. AOD values
213 were restricted to the range 0–5 to exclude extreme outliers.

214 **2.5 Correlation and multivariate regression analysis**

215 To quantify the influence of forest fires on aerosol loading, linear regressions of
216 the form $AOD = a + k \times \log_{10}[\text{fires}]$ applied separately to FAOD and CAOD. The
217 regression slope (k) represents fire sensitivity, with larger values indicating stronger
218 aerosol responses to fire activity. The $\log_{10}[\text{fires}]$ was adopted as the explanatory
219 variable, following common practice in wildfire research (Zhao et al., 2024; Abatzoglou
220 and Williams, 2016). We applied linear regressions to individual $1^\circ \times 1^\circ$ grid cells that
221 contained no fewer than 10 fire observations. Where statistically significant
222 associations were identified ($p < 0.05$), both the slope parameter (k) and the
223 corresponding R^2 values were mapped to illustrate their spatial variability. Differences
224 in regression slopes among grid cells were evaluated using two-tailed t tests.

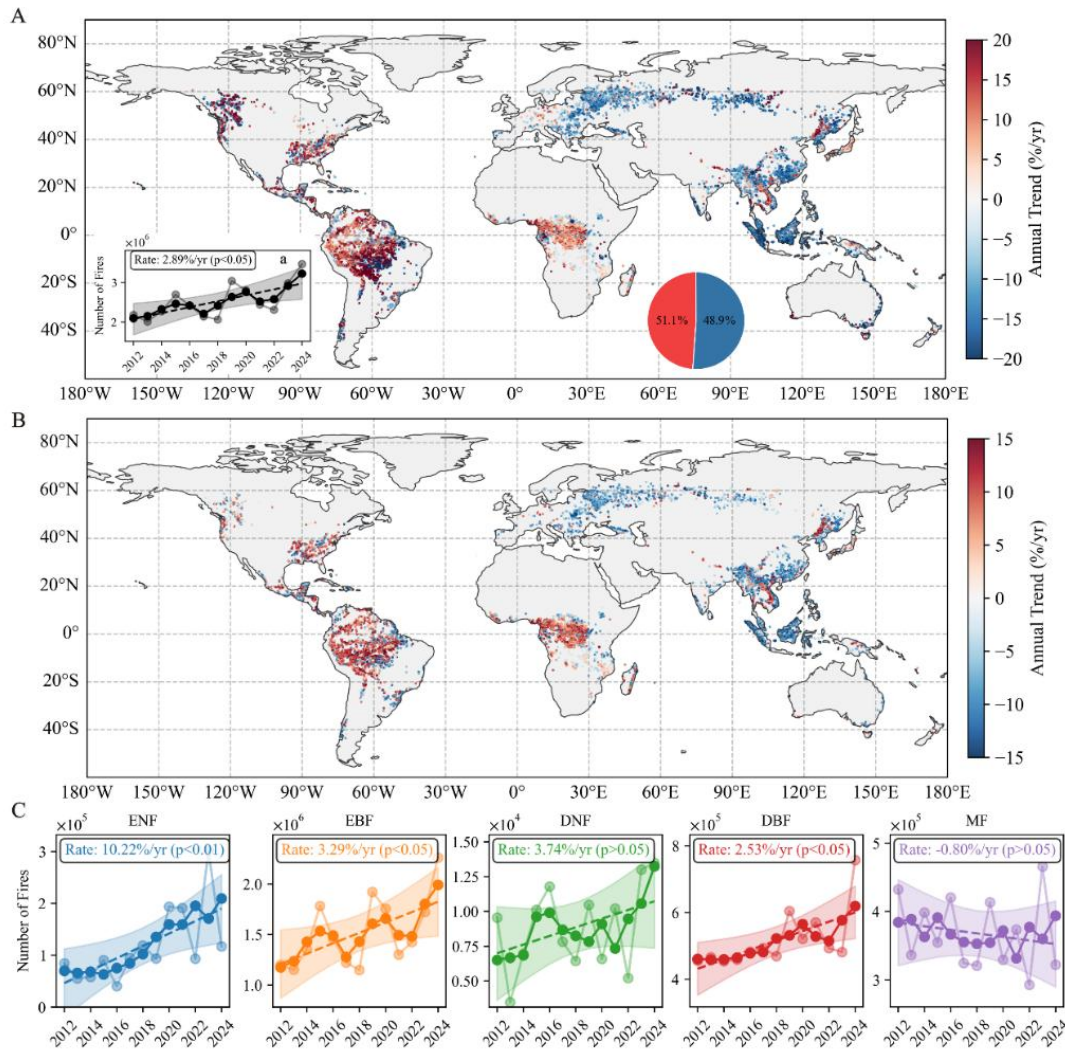
225 For the elevation-based analysis of forest fire activity, all monthly fire,
226 meteorological, vegetation, and topographic variables were spatially resampled to a 1°
227 $\times 1^\circ$ grid. For each grid cell, multiple linear regression model was conducted with
228 $\log_{10}[\text{fires}]$ as the response variable and FWI, leaf area index (LAI), 2mT, 10mW, and
229 daily maximum total precipitation as predictors. Year and month were additionally
230 included to represent long-term trends and seasonal variability. We employed ordinary
231 least squares (OLS) models to obtain baseline relationships, and statistical inference
232 was conducted using heteroskedasticity-robust standard errors ($p < 0.05$). To mitigate
233 multicollinearity among predictors, ridge regression with L_2 regularization was
234 additionally applied after standardizing all variables, with the optimal regularization
235 parameter selected via cross-validation. Variance inflation factors (VIFs) were
236 calculated to diagnose collinearity, and partial correlation analysis was applied to
237 isolate the independent effects of each driver after accounting for temporal influences.
238 Regression coefficients and model performance metrics were subsequently summarized
239 within elevation bins to characterize altitude-dependent fire–environment relationships.

240 **3. Results and discussion**

241 **3.1 Spatiotemporal patterns of forest fires and AOD**

242 Analysis of satellite-derived fire pixel counts across global forested regions from

243 2012 to 2024 reveals a modest but statistically significant increasing trend. Spatially,
244 51.1% of forest grid cells exhibit positive trends, exceeding the 48.9% showing
245 negative trends, with a global mean linear increase of 2.89% yr⁻¹ ($p < 0.05$, Figure 1A).
246 Our results indicate a growing number of forest fires, in agreement with the previously
247 reported global increase in forest burned area and mean fire pixel counts over last two
248 decades (Zheng et al., 2021; Yu and Ginoux, 2022). Geographically, significant positive
249 trends in fire pixel counts are concentrated in North America, northern South America,
250 and central Africa, whereas predominantly negative trends occur in Southeast Asia,
251 western and central Siberia, and eastern Europe (Figure 1A). The spatial patterns
252 derived from linear regression are consistent with those identified using the Mann-
253 Kendall test (Figure 1B). Notably, regions exhibiting increasing trends largely overlap
254 with areas of enhanced burned area and fire-driven carbon emissions in the tropical
255 moist broadleaf forest pyrome identified by Jones et al. (2024) for the period 2001–
256 2023. Increasing fire activity has also been reported in selected extratropical forest
257 ecoregions, including Canada (Wang et al., 2025) and Northeast China (Liu et al., 2023).



258

259 Figure 1. Global trends in forest fire occurrence during 2012–2024. (A) Spatial distribution of
 260 statistically significant ($p < 0.05$) trends in annual fire pixel counts. The inset (a) shows the
 261 corresponding global time series, including annual values (light circles), a 3-year centered moving
 262 average (dark circles), and the fitted linear trend with its 95% confidence interval (dashed line and
 263 shaded envelope). The accompanying pie chart summarizes the relative fractions of increasing (red)
 264 and decreasing (blue) trends. (B) Significant spatial changes in yearly fire frequency, with
 265 significance assessed by the Mann–Kendall test and slope magnitudes estimated using the Theil–
 266 Sen method. (C) Distribution of significant interannual trends by dominant forest type, using the
 267 same smoothing and trend analysis as in (a). ENF, evergreen needleleaf forest; EBF, evergreen
 268 broadleaf forest; DNF, deciduous needleleaf forest; DBF, deciduous broadleaf forest; MF, mixed
 269 forest.

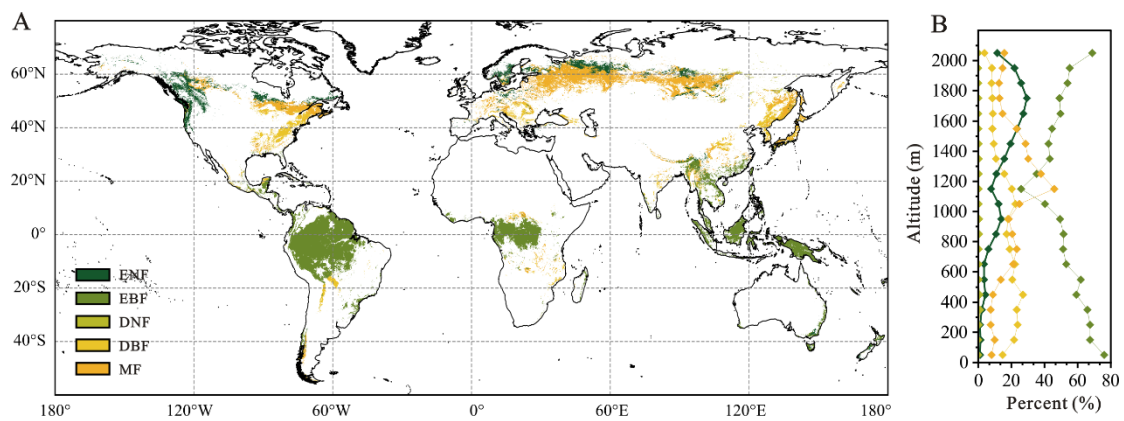
270

271

272

Considerable heterogeneity in fire activity is found across forest types. EBF
 accounts for the largest proportion of fire pixel counts globally, whereas ENF exhibits
 the strongest positive trend in fire occurrence (Figure 1C). By comparison, no

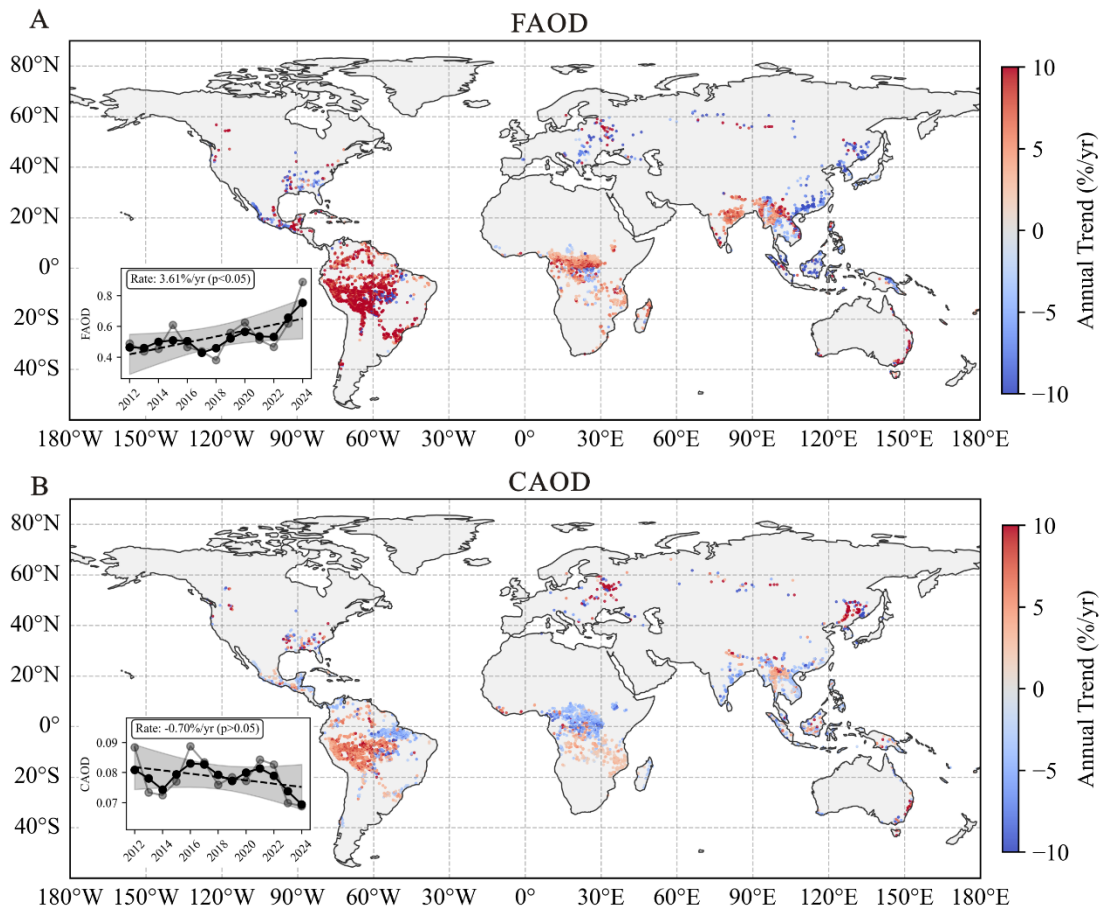
273 statistically significant changes are observed for DNF and MF. These forest types are
 274 primarily distributed across western and central Siberia (Figure 2A), regions
 275 characterized by declining fire activity (Figure 1A). Fire occurrence and severity are
 276 strongly mediated by vegetation characteristics, including forest type and fuel structure
 277 (Wang et al., 2025). High fire frequency and density are commonly associated with
 278 evergreen needleleaf forests, such as those dominated by Chir pine (*Pinus roxburghii*),
 279 which are characterized by high-intensity fire regimes (Kumar and Kumar, 2022). This
 280 elevated fire susceptibility is attributed to needle-shaped foliage, high resin content, and
 281 ladder-like branch architecture, which collectively enhance fuel flammability and
 282 vertical fire spread (Alexander and Cruz, 2011; Wang et al., 2025).



283
 284 Figure 2. Forest classification and its topographic variation. (A) Spatial patterns of the dominant
 285 forest categories. (B) Elevation-dependent distribution of forest cover, expressed as the percentage
 286 area occupied by each type within individual elevation bands. ENF, evergreen needleleaf forest;
 287 EBF, evergreen broadleaf forest; DNF, deciduous needleleaf forest; DBF, deciduous broadleaf forest;
 288 MF, mixed forest.

289 Aerosols influence the atmospheric radiation balance through the scattering and
 290 absorption of radiation (Andreae et al., 2004; Blanchard-Wrigglesworth et al., 2025).
 291 Owing to their distinct optical properties, different aerosol types exert varying climatic
 292 effects (Lin et al., 2021), particularly between fine-mode and coarse-mode particles (Li
 293 et al., 2025). To better investigate aerosol responses to forest fire activity, aerosol
 294 loading is therefore characterized using FAOD and CAOD. A consistent positive
 295 association between FAOD and fire pixel counts is observed across global forest
 296 regions from 2012 to 2024, whereas no comparable trend is detected for CAOD (Figure

3) It should be noted that FAOD and CAOD may also be influenced by aerosol sources unrelated to wildfire emissions; therefore, the comparison with fire activity should be treated as a first-order diagnostic of their potential linkage rather than a strict attribution of aerosol sources. The fire–FAOD relationship was quantified using linear regression of the form $(FAOD = a + k_F \times \log_{10}[\text{fires}])$ applied to each $1^\circ \times 1^\circ$ grid cell. Widespread statistically significant positive k_F values indicate that fine-mode particles dominate wildfire-related aerosol loading (Figure 4A), consistent with previous evidence that biomass burning predominantly contributes to the fine-mode portion of the aerosol population (Yan et al., 2024; Yang et al., 2021b; Kaskaoutis et al., 2014; Pei et al., 2025).

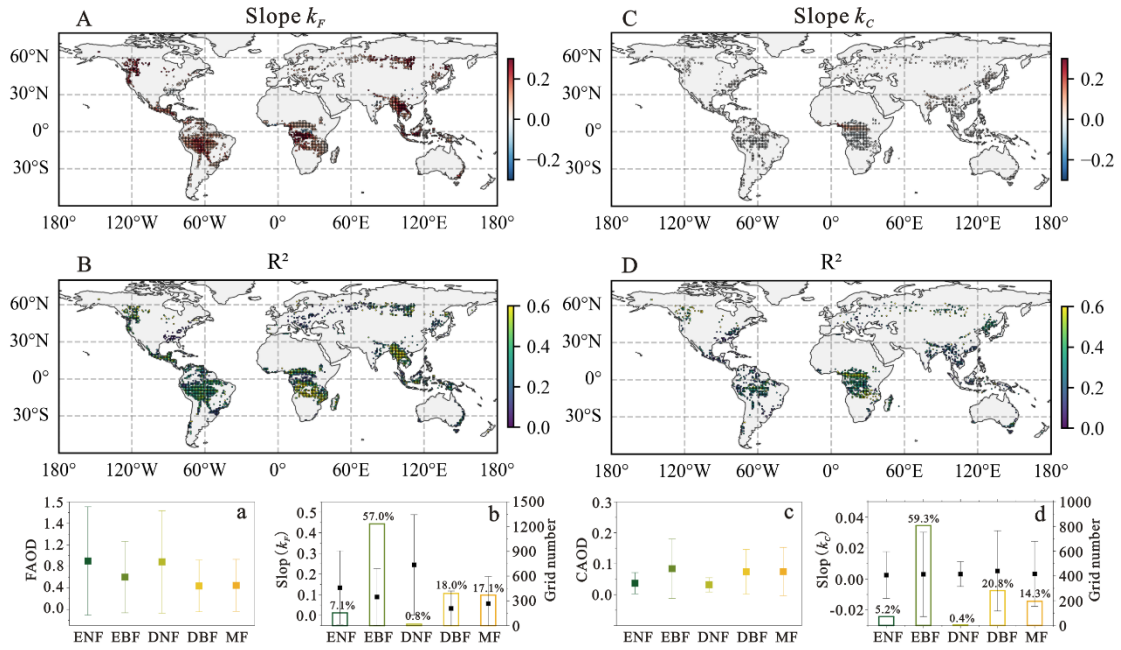


306
307 Figure 3. Spatiotemporal trends in FAOD and CAOD during 2012–2024. (A) Spatial distribution of
308 statistically significant trends ($p < 0.05$) in FAOD. (B) Corresponding distribution for CAOD. Insets
309 show the annual global time series, including annual values (light circles), a 3-year centered moving
310 average (dark circles), and the linear trend with its 95% confidence interval (dashed line with
311 shading).

312 The k_F slope values exhibited variation across forest types, with the highest values

313 magnitude observed in DNF (0.25 ± 0.24), followed by ENF (0.13 ± 0.18), EBF (0.09
314 ± 0.14), MF (0.06 ± 0.13) and DBF (0.03 ± 0.08) (Figure 4b). This ranking is consistent
315 with the spatial pattern of average FAOD across these forest types (Figure 4a). Such
316 differences can be attributed to species-dependent emission strengths, as dominant taxa
317 contribute unevenly to wildfire-derived aerosols. For example, within ENF regions,
318 *Pseudotsuga* and *Picea* account for 15% and 71.1% of total FAOD contribution from
319 wildfire, respectively; among broadleaf forests, the genus *Quercus* alone contributes
320 50.6% (Chen et al., 2025). These patterns underscore that aerosol emissions from forest
321 fires depend not only on burned areas but also on fuel type and combustion efficiency
322 (Keywood et al., 2013). In contrast, no significant positive k_C values are detected for
323 CAOD (Figure 4C). The average of k_C values in different forest types was close to 0
324 with minimal variation (Figure 4d), indicating the absence of a systematic forest fire
325 influence on coarse-mode aerosol loading. In contrast to the large aerosol particles
326 associated with large fire events, such as pyroCb emissions (Li et al., 2025) or coarse
327 dust produced by post-fire dust outbreaks caused by reduced vegetation cover and soil
328 moisture (Yu and Ginoux, 2022), the results presented here mainly represent the global
329 mean response within forest fire regions. Although large fire events may generate
330 unusually high aerosol loading or coarse-mode dust, such episodic events are not fully
331 captured in the large-scale averages analyzed in this study.

332



333

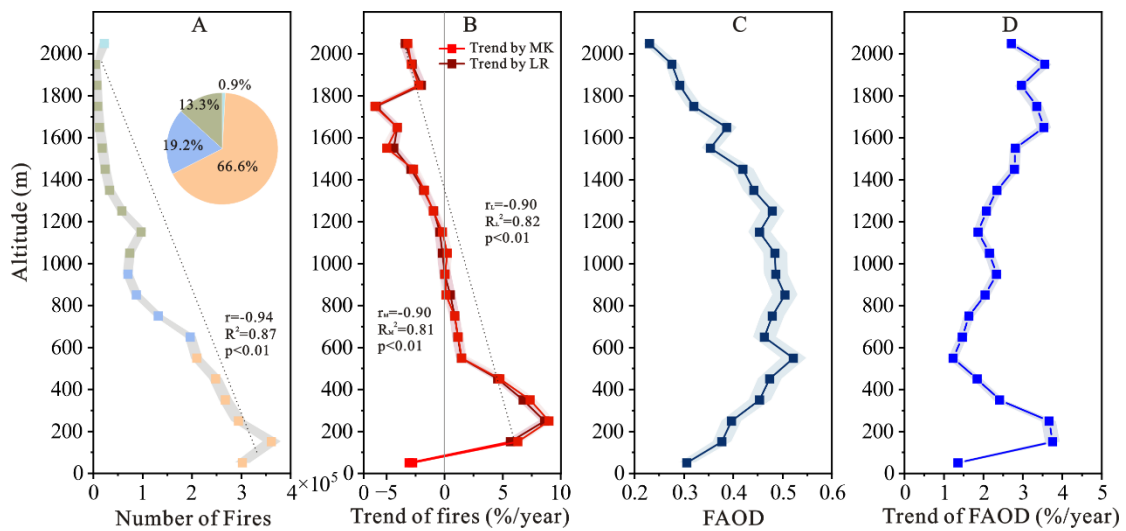
334 Figure 4. Correlation analysis between forest fires and AOD. (A, B) Regression slope k_F and R^2 for
 335 FAOD-fire relationship. (C, D) Slope k_C and R^2 for CAOD-fire relationship. (a, b) Forest-type
 336 averages of FAOD and Slope k_F . (c, d) Forest-type averages of CAOD and Slope k_C . Maps (A-D)
 337 show only locally significant relationships (linear regression, $p < 0.05$). Error bars in panels (a-d)
 338 denote standard errors. In panels (b) and (d), bar height indicates the number of grid cells per forest
 339 type, with numbers above bars showing the fractional area contribution of each forest type. ENF,
 340 evergreen needleleaf forest; EBF, evergreen broadleaf forest; DNF, deciduous needleleaf forest;
 341 DBF, deciduous broadleaf forest; MF, mixed forest.

342 3.2 Elevation-Dependent Patterns of Forest Fire Occurrence and FAOD

343 To evaluate how topography shapes forest fire activity globally, we examined the
 344 elevational dependence of fire occurrence from 2012 to 2024. A clear and statistically
 345 significant decline in mean annual fire pixel counts with increasing elevation was
 346 identified (Figure 5A). Forest fires were predominantly concentrated at low elevations,
 347 with 66.6% of total fire detections occurring below 600 m, followed by 19.2% between
 348 601 and 1000 m and 13.3% between 1001 and 2000 m. Only 0.9% of fires were detected
 349 above 2000 m (Figure 5A). This inverse relationship between elevation and fire activity
 350 agrees with previous regional studies conducted in the Canadian Rocky Mountains
 351 (Rogean and Armstrong, 2017) and across forested regions of China (Tian et al., 2013;
 352 Ma et al., 2020). Similar elevational dependence is also evident in the interannual trends.
 353 Both the multiyear mean fire pixel counts, and the corresponding annual trends exhibit

354 a pronounced decrease from low to high elevations (Figure 5A, B). However, Xu and
 355 You (2022) reported increasing burned areas in global high-mountain regions above
 356 3000 m, primarily focusing on high-mountain ecosystems that include alpine and other
 357 non-forest environments. In contrast, the present study examines wildfire activity
 358 within global forest regions, where most fires occur at low and mid elevations.
 359 Differences in vegetation type, fuel availability, and fire regimes between forested
 360 landscapes and alpine environments may partly explain these contrasting patterns.

361 Notably, while the largest absolute number of fires were observed between 100
 362 and 200 m, the strongest positive trend in fire activity occurred near ~300 m before
 363 declining at higher elevations. This discrepancy suggests that recent fire activity has
 364 increasingly concentrated around the ~300 m elevation range, potentially reflecting the
 365 combined influence of climate variability and fire management practices. In contrast, a
 366 weak negative trend in fire occurrence was observed below 100 m, which may be
 367 associated with more effective control of ignition sources in densely managed lowland
 368 regions (Wang et al., 2022b).



369
 370 Figure 5. Elevational variations in multiyear mean fire pixel counts, FAOD, and their temporal
 371 trends. (A, B) Multiyear mean (A) and significant annual trend (B) in fire pixel counts as a function
 372 of elevation. (C, D) Corresponding multiyear average (C) and trend (D) in FAOD. Dashed lines
 373 indicate overall elevation-dependent tendencies in (A) and (B). Colors denote elevation classes: 0–
 374 600 m (light orange), 600–1000 m (light blue), 1000–2000 m (gray-green), and >2000 m (light
 375 cyan). Shaded areas represent the 95% confidence intervals.

376 In contrast to the monotonic decline in fire occurrence, FAOD exhibits a distinct
377 elevational pattern. While FAOD trends below 600 m broadly track those of fire activity,
378 its multiyear mean values peak at mid-elevations (600–1400 m) rather than at low
379 elevations (Figure 5C, D). This divergence indicates that FAOD is not solely controlled
380 by local fire occurrence but is also influenced by forest composition and
381 topographically modulated by smoke transport processes. Around 600 m elevation,
382 forest composition shifts toward a higher fraction of ENF (Figure 2B), which exhibits
383 stronger FAOD sensitivity to fire activity ($k_F = 0.14 \pm 0.18$) than EBF ($k_F = 0.09 \pm 0.14$).
384 In addition, smoke particles released by low-elevation fires may be carried to higher
385 levels of the atmosphere via aerosol self-lifting processes associated with radiative
386 heating and convective motions (De Laat et al., 2012; Ohneiser et al., 2023; Xu et al.,
387 2025), thus elevating FAOD levels at mid-elevations. Above 600 m, the strengthening
388 FAOD trends with elevation diverge from the concurrent decline in fire occurrence,
389 implying the involvement of additional processes beyond local fire emissions. In
390 addition, with fewer than 50 grid cells above 1500 m exhibiting statistically significant
391 trends, the representativeness and accuracy of the computed global FAOD trend may
392 be compromised. Collectively, these results suggest that mid-elevation regions (600–
393 1400 m) are disproportionately influenced by smoke aerosols from forest fires at a
394 global scale.

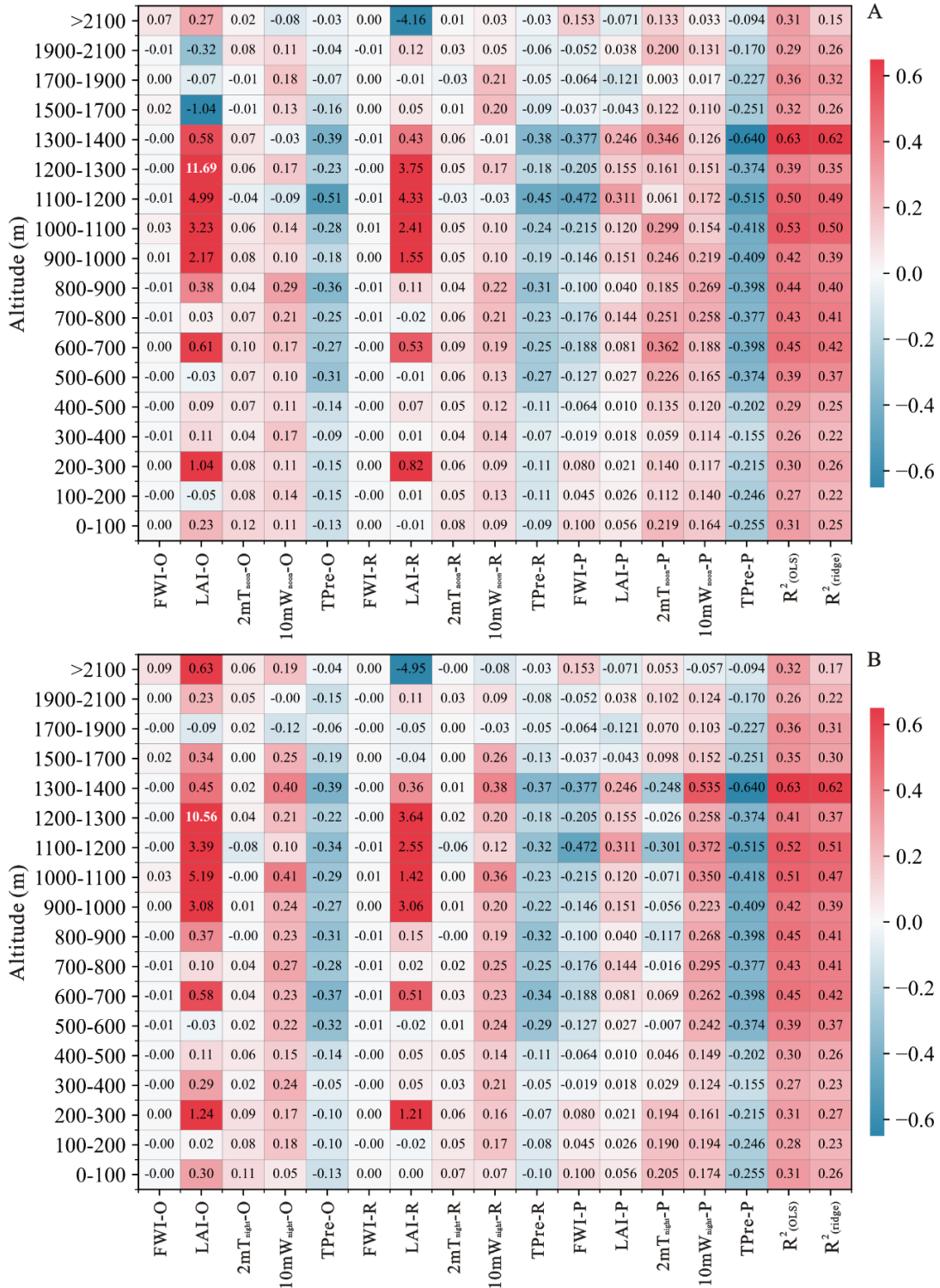
395 **3.3 Drivers of Elevational-Dependent Variations in Fire Activity**

396 To explain the contrasting elevational patterns of forest fire occurrence identified
397 in Section 3.2, we next examine the meteorological and ecological drivers governing
398 fire activity along with the elevation gradient. Vegetation fire activity is governed by
399 multiple interacting factors, including ignition sources, fuel supply and moisture, fire-
400 conducive weather, and forest management practices (Wang et al., 2022a; Clarke et al.,
401 2025). However, the relative contributions of these drivers change with elevation.
402 Notably, the FWI—often used to characterize the meteorological fire danger—exerts
403 little explanatory power, with regression coefficients near zero at all heights (Figure 6).
404 Partial correlation coefficients were negative between 300 and 2100 m, indicating a

405 weak association between FWI and fire occurrence after accounting for elevation. The
406 weak agreement observed here aligns with earlier reports (Su et al., 2025; Wang et al.,
407 2025) and arises primarily from mismatches in spatial and temporal resolution. FWI
408 primarily represents short-term surface meteorological conditions conducive to
409 wildfire occurrence, but it does not explicitly account for atmospheric instability, which
410 can play an important role in the development of large fires (Pinto et al., 2020). In
411 addition, our analysis focuses on the influence of topographic effects. The complex
412 regional topography may strongly modulate atmospheric instability (Santos et al., 2023),
413 which is closely associated with lightning activity and has been shown to be an
414 important factor in fire growth at the local scale (Haines, 1988).

415 To further disentangle elevational controls on fire activity, we examined individual
416 climatic and ecological variables associated with fuel aridity, ignition potential, and fuel
417 availability. Observed declines in LAI and wind speed with increasing elevation (Figure
418 7) are consistent with a reduced probability of fire occurrence at higher altitudes. LAI
419 was selected as a proxy for fuel availability (Yu et al. 2020). Multiple linear regression
420 analyses reveal pronounced elevation-dependent relationships (Figure 6). At high
421 elevations (>1500 m), fire occurrence shows no significant relationship with LAI. In
422 contrast, fire activity shows clear positive correlations with LAI at both low (200–300
423 m) and mid-elevations (600–1400 m), highlighting the importance of vegetation density
424 as a proxy for available fuels. While relatively strong regression coefficients are
425 observed in the low-elevation band (200–300 m), the corresponding R^2 values are
426 comparatively low, indicating that LAI explains only a limited fraction of the variability
427 in fire occurrence at these elevations. Consequently, the relationship between
428 vegetation and fire activity is more robust at mid-elevations. Although ridge regression
429 produced smaller coefficients than OLS, the coefficient for LAI remained significantly
430 higher than those of the other predictors. These observations support earlier studies
431 showing that vegetation structure and forest composition strongly regulate fire
432 dynamics (Parks et al., 2018; Wang et al., 2022c). In particular, evergreen needleleaf
433 species such as *Pinus densiflora* and *Pinus roxburghii* possess resin-rich needles that

434 enhance flammability and promote high-intensity fire behavior (Baek et al., 2022;
 435 Kumar and Kumar, 2022).



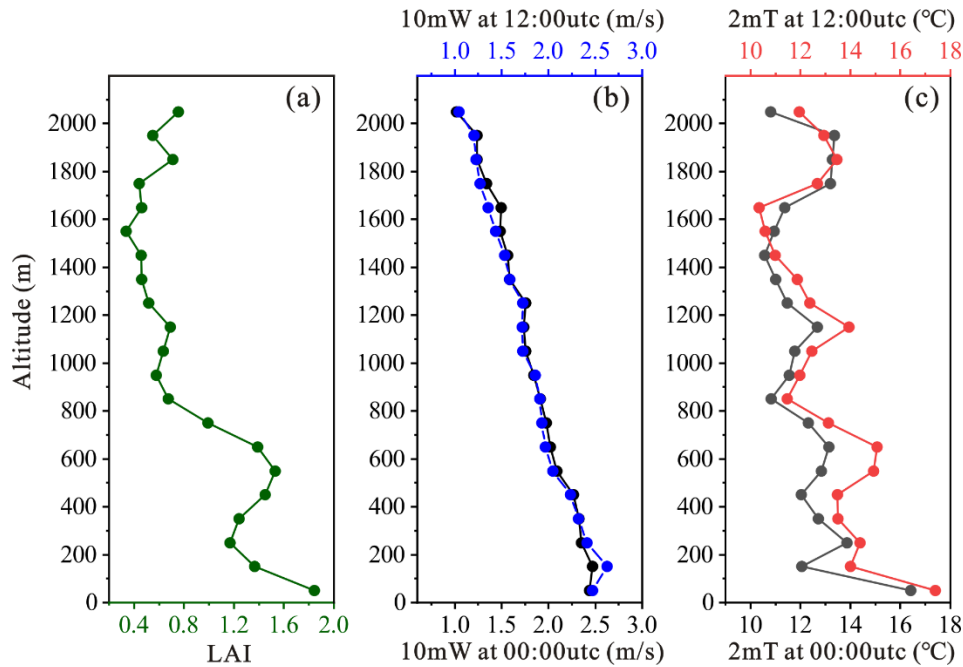
436
 437 Figure 6. Elevational variations in the key drivers of fire activity derived from multiple linear
 438 regression. Fire pixel counts were related to the FWI, LAI, 2mT, 10mW, and maximum total
 439 precipitation (TPre) ($p < 0.05$). Panels (A) and (B) represent nighttime and midday conditions,
 440 respectively. For each predictor, “-O” denotes the OLS standardized coefficient, “-R” the ridge

441 regression coefficient, and “-P” the partial correlation coefficient. Model skill was evaluated using
442 the coefficients of determination derived from both OLS ($R^2_{(OLS)}$) and ridge regression ($R^2_{(ridge)}$).

443 Air temperature, closely linked to climate change, influences fire activity by
444 modulating fuel drying and convective processes (Dastour et al., 2024; Duane et al.,
445 2021). However, temperature exhibited negligible effects, with both OLS and ridge
446 coefficients remaining close to zero across all elevations under both nighttime and
447 midday conditions. The weak elevational dependence of 2 m air temperature (Figure 7)
448 suggests that temperature alone cannot explain the observed decline in fire occurrence.
449 At mid-elevations, nighttime temperature exhibits a weak negative partial correlation
450 with fire occurrence, while daytime temperature shows a positive association,
451 highlighting the complex and diurnally dependent influence of temperature under
452 topographic constraints. In contrast, precipitation emerges as a robust suppressor of fire
453 activity across all elevation bands, with the strongest effects observed at mid-elevations.
454 The consistently negative regression coefficients indicate that precipitation deficits are
455 a primary determinant of fire occurrence and spatial distribution, consistent with
456 previous findings linking fire activity to precipitation amount and rainy-day frequency
457 (Kim et al., 2025). Relative humidity likely reinforces this effect by further modulating
458 fuel moisture, particularly in boreal forest systems (Veraverbeke et al., 2017; Dastour
459 et al., 2024).

460 Wind speed also exhibits strong elevational dependence. Nighttime wind speed
461 shows a positive association with fire occurrence below 1800 m in both OLS and ridge
462 models, with the strongest influence at mid-elevations (Figure 6). Daytime wind speed
463 is positively related to fire activity at low elevations but shows no significant
464 relationship at mid-elevations, likely reflecting differences between daytime up-valley
465 winds and nighttime downslope flows. In mountainous terrain, downslope flows may
466 advect warm and dry air toward lower elevations, creating fire-favorable conditions
467 when fuels are sufficiently dry (Abatzoglou et al., 2023; Abatzoglou et al., 2021).
468 Partial correlation analyses indicate that, when isolated from other factors, wind speed
469 remains positively associated with fire activity across elevations below 2000 m,

470 particularly at mid-elevations. Elevated wind speeds enhance fire activity by increasing
 471 evaporative drying, promoting sustained combustion, and facilitating ember transport
 472 (Ma et al., 2020; Jones et al., 2022).



473
 474 Figure 7. Elevation patterns of multiyear mean variables. (a) Leaf area index (LAI). (b) 10 m wind
 475 speed (10mW) at 00:00 and 12:00 utc. (c) 2 m air temperature (2mT) at 00:00 utc and 12:00 utc.

476 Together, these results identify precipitation, wind speed, and vegetation
 477 abundance as primary drivers of the elevation-dependent distribution of forest fires. At
 478 mid-elevations, fire activity is jointly controlled by sufficient fuel availability and
 479 aridity, the latter mediated by reduced precipitation and elevation-specific wind regimes.
 480 In addition, enhanced FAOD associated with fire-emitted smoke aerosols—dominated
 481 by light-absorbing black carbon (Yu et al., 2019)—may further contribute to
 482 atmospheric heating and fuel drying at seasonal to interannual timescales (Pei et al.,
 483 2025), potentially reinforcing fire-favorable conditions. Several potentially important
 484 drivers, including anthropogenic ignitions, lightning frequency, soil moisture, and
 485 regional fire management practices, were not explicitly considered in this analysis. In
 486 addition, the limited number of grid cells (< 10) between 1300 and 2100 m reduces
 487 statistical robustness, suggesting that fire controls at these elevations may be more
 488 complex at the global scale. This threshold differs from that used in the FAOD trend
 489 analysis because the two analyses are conducted at different spatial resolutions.

490 Specifically, the FAOD trend analysis is based on a 0.1° grid with a large number of
491 global grid cells, for which a threshold of 50 grid cells is applied to ensure statistical
492 representativeness. In contrast, the elevation-dependent regression analysis is
493 performed on a coarser 1° grid, where the number of available grid cells is substantially
494 smaller; therefore, a lower threshold of 10 grid cells is adopted to maintain sufficient
495 statistical robustness. These unaccounted factors likely contribute to the residual
496 variability in fire occurrence and warrant further investigation.

497 **4. Conclusion**

498 Across global forested regions from 2012 to 2024, we analyze spatiotemporal
499 variability in forest fire activity and its associated AOD, together with their elevation-
500 dependent drivers, across global forested regions during 2012–2024. Satellite
501 observations reveal a modest but statistically significant increase in forest fire
502 occurrence, with a global mean linear trend of $+2.89\% \text{ yr}^{-1}$. Fire trends vary
503 substantially among forest types, with ENF exhibiting the strongest positive trends,
504 while DNF and MF show no significant changes. Fire-associated aerosol loading is
505 dominated by fine-mode particles. The consistent positive trends and statistically
506 significant relationships between FAOD and fire pixel counts, together with the absence
507 of a corresponding response in CAOD, indicate that forest fire emissions primarily
508 enhance the fine aerosol fraction. Both the multiyear mean fire pixel counts and its
509 temporal trend decline systematically with increasing elevation, from lowlands to
510 elevations above 2000 m, highlighting a pronounced elevational control on global forest
511 fire activity. In contrast, FAOD exhibits a more complex elevational structure. Below
512 600 m, FAOD trends broadly track fire occurrence, whereas at mid-elevations (600–
513 1400 m) FAOD displays elevated mean values and increasing trends despite declining
514 fire occurrence. This divergence suggests that mid-elevation aerosol burdens are
515 influenced not only by local fire activity but also by shifts in forest-type composition
516 and by topographically modulated smoke transport, including aerosol self-lifting driven
517 by radiative absorption and atmospheric convection.

518 Elevation-stratified multiple linear regression analyses further indicate that forest

519 fire activity is primarily controlled by the combined effects of fuel availability and
520 aridity. Fuel load, represented by leaf area index, plays a critical role at mid-elevations,
521 while precipitation consistently exerts a suppressive influence on fire occurrence across
522 all elevation bands. Wind speed emerges as an important contributor to fuel drying and
523 fire spread, especially in mid-elevation regions. In contrast, temperature and the FWI
524 show limited independent explanatory power once elevation and other covarying
525 factors are considered. Overall, these results highlight elevation as an important
526 organizing dimension linking forest fire activity, aerosol emissions, and their
527 underlying drivers at the global scale. By elucidating how fuel characteristics,
528 meteorological conditions, and topography jointly regulate fire–aerosol interactions
529 across elevation gradients, this study provides a physically grounded framework for
530 improving wildfire risk assessment, interpreting fire-driven aerosol impacts, and
531 refining fire management strategies under a changing climate. Continued investigation
532 incorporating anthropogenic ignitions, lightning activity, and region-specific
533 management practices will be essential for further constraining elevation-dependent
534 fire regimes.

535

536 **Data availability**

537 Active fire detections at 375 m resolution were obtained from the NASA Land-SIPS
538 VIIRS product, provided through the Fire Information for Resource Management
539 System (FIRMS) (<https://earthdata.nasa.gov/firms>). Elevation information was derived
540 from the 2024 General Bathymetric Chart of the Oceans (GEBCO) global gridded
541 dataset (doi:10.5285/1c44ce99-0a0d-5f4f-e063-7086abc0ea0f), available at
542 <https://www.gebco.net/>. Land cover classifications were taken from the MODIS Land
543 Cover Type Yearly Climate Modeling Grid (CMG; MCD12Q1), distributed via the
544 Level-1 and Atmosphere Archive & Distribution System (LAADS DAAC)
545 (<https://ladsweb.modaps.eosdis.nasa.gov/search/order/1>). Historical Fire Weather
546 Index (FWI) data were sourced from the Copernicus Emergency Management Service
547 (<https://doi.org/10.24381/cds.0e89c522>). Meteorological variables and leaf area index
548 (LAI) were extracted from the ECMWF Reanalysis v5 (ERA5) archive
549 (<https://cds.climate.copernicus.eu/datasets>). The daily global FAOD and CAOD
550 datasets at 500 nm are available from the authors upon request.

551

552 **Author contributions**

553 CZ initiated and supervised the study. QP carried out the data analysis and drafted the
554 initial manuscript. XY contributed the daily global FAOD and CAOD datasets. All
555 authors (CZ, QP, XY, XY, AC, and XW) participated in improving the manuscript.

556

557 **Competing interests**

558 The authors declare that they have no conflict of interest.

559

560 **Acknowledgments**

561 This work is supported by the Yunnan Provincial Science and Technology Project at
562 Southwest United Graduate School (grant number 202302AP370003). We are deeply
563 appreciative of MODIS, GEBCO, ECMWF and NASA's FIRMS teams for granting
564 access to their valuable data.

565

566 **References**

- 567 Abatzoglou, J. T. and Williams, A. P.: Impact of anthropogenic climate change on wildfire across western
568 US forests, *P Natl Acad Sci USA*, 113, 11770-11775, 10.1073/pnas.1607171113, 2016.
- 569 Abatzoglou, J. T., Rupp, D. E., O'Neill, L. W., and Sadegh, M.: Compound Extremes Drive the Western
570 Oregon Wildfires of September 2020, *Geophysical Research Letters*, 48, e2021GL092520, ARTN
571 e2021GL092520.1029/2021GL092520, 2021.
- 572 Abatzoglou, J. T., Kolden, C. A., Williams, A. P., Sadegh, M., Balch, J. K., and Hall, A.: Downslope
573 Wind-Driven Fires in the Western United States, *Earths Future*, 11, e2022EF003471, ARTN
574 e2022EF003471.1029/2022EF003471, 2023.
- 575 Abatzoglou, J. T., Kolden, C. A., Cullen, A. C., Sadegh, M., Williams, E. L., Turco, M., and Jones, M.
576 W.: Climate change has increased the odds of extreme regional forest fire years globally, *Nature*
577 *Communications*, 16, 6390, ARTN 6390.1038/s41467-025-61608-1, 2025.
- 578 Alexander, M. E. and Cruz, M. G.: Crown fire dynamics in conifer forests, in: *Synthesis of Knowledge*
579 *of Extreme Fire Behavior*, 107-142, 2011.
- 580 Andela, N., Morton, D. C., Giglio, L., Chen, Y., van der Werf, G. R., Kasibhatla, P. S., DeFries, R. S.,
581 Collatz, G. J., Hantson, S., Kloster, S., Bachelet, D., Forrest, M., Lasslop, G., Li, F., Mangeon, S.,
582 Melton, J. R., Yue, C., and Randerson, J. T.: A human-driven decline in global burned area, *Science*,
583 356, 1356-1361, 10.1126/science.aal4108, 2017.
- 584 Andreae, M. O., Rosenfeld, D., Artaxo, P., Costa, A. A., Frank, G. P., Longo, K. M., and Silva-Dias, M.
585 A. F.: Smoking rain clouds over the Amazon, *Science*, 303, 1337-1342, DOI
586 10.1126/science.1092779, 2004.
- 587 Baek, S., Lim, J., and Kim, W.: Analysis on the Fire Progression and Severity Variation of the Massive
588 Forest Fire Occurred in Uljin, Korea, 2022, *Forests*, 13, 2185, ARTN 2185.10.3390/f13122185, 2022.
- 589 Birch, D. S., Morgan, P., Kolden, C. A., Abatzoglou, J. T., Dillon, G. K., Hudak, A. T., and Smith, A. M.
590 S.: Vegetation, topography and daily weather influenced burn severity in central Idaho and western
591 Montana forests, *Ecosphere*, 6, art17, Artn 17.10.1890/Es14-00213.1, 2015.

592 Blanchard-Wrigglesworth, E., DeRepentigny, P., and Frierson, D. M. W.: Increasing boreal fires reduce
593 future global warming and sea ice loss, *Proceedings of the National Academy of Sciences*, 122,
594 e2424614122, 10.1073/pnas.2424614122, 2025.

595 Bowman, D. M. J. S., Balch, J. K., Artaxo, P., Bond, W. J., Carlson, J. M., Cochrane, M. A., D'Antonio,
596 C. M., DeFries, R. S., Doyle, J. C., Harrison, S. P., Johnston, F. H., Keeley, J. E., Krawchuk, M. A.,
597 Kull, C. A., Marston, J. B., Moritz, M. A., Prentice, I. C., Roos, C. I., Scott, A. C., Swetnam, T. W.,
598 van der Werf, G. R., and Pyne, S. J.: Fire in the Earth System, *Science*, 324, 481-484,
599 10.1126/science.1163886, 2009.

600 Canadell, J. G., Meyer, C. P., Cook, G. D., Dowdy, A., Briggs, P. R., Knauer, J., Pepler, A., and Haverd,
601 V.: Multi-decadal increase of forest burned area in Australia is linked to climate change, *Nature*
602 *Communications*, 12, 6921, ARTN 692110.1038/s41467-021-27225-4, 2021.

603 Chen, J. Y., Chen, H. W., Li, Z. Q., Wang, Q., Wang, G. Q., Jia, K., and Yan, X.: Divergent radiative
604 forcing of fine-mode aerosols across tree genera during wildfires in North America and Europe,
605 *Journal of Hazardous Materials*, 495, 138881, ARTN 13888110.1016/j.jhazmat.2025.138881, 2025.

606 Clarke, H., Di Giuseppe, F., Johnston, L., Marlon, J., Penman, T., Pitman, A. J., van der Werf, G. R., and
607 Flannigan, M. D.: Gazing into the flames: A guide to assessing the impacts of climate change on
608 landscape fire, *Science Advances*, 11, eadz2429, ARTN eadz242910.1126/sciadv.adz2429, 2025.

609 Cunningham, C. X., Williamson, G. J., and Bowman, D. M. J. S.: Increasing frequency and intensity of
610 the most extreme wildfires on Earth, *Nature Ecology & Evolution*, 8, 1420-1425, 10.1038/s41559-
611 024-02452-2, 2024.

612 Dastour, H., Ahmed, M. R., and Hassan, Q. K.: Analysis of forest fire patterns and their relationship with
613 climate variables in Alberta's natural subregions, *Ecological Informatics*, 80, 102531, ARTN
614 10253110.1016/j.ecoinf.2024.102531, 2024.

615 de Laat, A. T. J., Stein Zweers, D. C., Boers, R., and Tuinder, O. N. E.: A solar escalator: Observational
616 evidence of the self-lifting of smoke and aerosols by absorption of solar radiation in the February
617 2009 Australian Black Saturday plume, *Journal of Geophysical Research: Atmospheres*, 117,
618 10.1029/2011jd017016, 2012.

619 Duane, A., Castellnou, M., and Brotons, L.: Towards a comprehensive look at global drivers of novel
620 extreme wildfire events, *Climatic Change*, 165, 43, ARTN 4310.1007/s10584-021-03066-4, 2021.

621 Fan, H., Wang, Y., Zhao, C. F., Yang, Y. K., Yang, X. C., Sun, Y., and Jiang, S. Y.: The Role of Primary
622 Emission and Transboundary Transport in the Air Quality Changes During and After the COVID-
623 19 Lockdown in China, *Geophysical Research Letters*, 48, e2020GL091065, ARTN
624 e2020GL09106510.1029/2020GL091065, 2021.

625 Gatti, L. V., Basso, L. S., Miller, J. B., Gloor, M., Domingues, L. G., Cassol, H. L. G., Tejada, G., Aragao,
626 L. E. O. C., Nobre, C., Peters, W., Marani, L., Arai, E., Sanches, A. H., Corrêa, S. M., Anderson, L.,
627 Von Randow, C., Correia, C. S. C., Crispim, S. P., and Neves, R. A. L.: Amazonia as a carbon source
628 linked to deforestation and climate change, *Nature*, 595, 388+, 10.1038/s41586-021-03629-6, 2021.

629 Haines, D. A.: A lower atmospheric severity index for wildland fires, *National Weather Digest*, 13, 23-
630 27, 1988.

631 Hamilton, D. S., Perron, M. M. G., Bond, T. C., Bowie, A. R., Buchholz, R. R., Guieu, C., Ito, A.,
632 Maenhaut, W., Myriokefalitakis, S., Olgun, N., Rathod, S. D., Schepanski, K., Tagliabue, A.,
633 Wagner, R., and Mahowald, N. M.: Earth, Wind, Fire, and Pollution: Aerosol Nutrient Sources and
634 Impacts on Ocean Biogeochemistry, *Annual Review of Marine Science*, 14, 303-330,

635 10.1146/annurev-marine-031921-013612, 2022.

636 Harper, H. and Sandwell, D. T.: Global Predicted Bathymetry Using Neural Networks, *Earth and Space*

637 *Science*, 11, e2023EA003199, ARTN e2023EA00319910.1029/2023EA003199, 2024.

638 Huang, Y. H., Jin, Y. F., Schwartz, M. W., and Thorne, J. H.: Intensified burn severity in California's

639 northern coastal mountains by drier climatic condition, *Environmental Research Letters*, 15, 104033,

640 ARTN 10403310.1088/1748-9326/aba6af, 2020.

641 Jolly, W. M., Cochrane, M. A., Freeborn, P. H., Holden, Z. A., Brown, T. J., Williamson, G. J., and

642 Bowman, D. M. J. S.: Climate-induced variations in global wildfire danger from 1979 to 2013,

643 *Nature Communications*, 6, 7537, 10.1038/ncomms8537, 2015.

644 Jones, M. W., Veraverbeke, S., Andela, N., Doerr, S. H., Kolden, C., Mataveli, G., Pettinari, M. L., Le

645 Quéré, C., Rosan, T. M., van der Werf, G. R., van Wees, D., and Abatzoglou, J. T.: Global rise in

646 forest fire emissions linked to climate change in the extratropics, *Science*, 386, ARTN

647 ead1588910.1126/science.ad15889, 2024.

648 Jones, M. W., Abatzoglou, J. T., Veraverbeke, S., Andela, N., Lasslop, G., Forkel, M., Smith, A. J. P.,

649 Burton, C., Betts, R. A., van der Werf, G. R., Sitch, S., Canadell, J. G., Santín, C., Kolden, C., Doerr,

650 S. H., and Le Quéré, C.: Global and Regional Trends and Drivers of Fire Under Climate Change,

651 *Reviews of Geophysics*, 60, e2020RG000726, ARTN e2020RG00072610.1029/2020RG000726,

652 2022.

653 Kaskaoutis, D. G., Kumar, S., Sharma, D., Singh, R. P., Kharol, S. K., Sharma, M., Singh, A. K., Singh,

654 S., Singh, A., and Singh, D.: Effects of crop residue burning on aerosol properties, plume

655 characteristics, and long-range transport over northern India, *J Geophys Res-Atmos*, 119, 5424-

656 5444, 10.1002/2013jd021357, 2014.

657 Keywood, M., Kanakidou, M., Stohl, A., Dentener, F., Grassi, G., Meyer, C. P., Tørseth, K., Edwards, D.,

658 Thompson, A. M., Lohmann, U., and Burrows, J.: Fire in the Air: Biomass Burning Impacts in a

659 Changing Climate, *Critical Reviews in Environmental Science and Technology*, 43, 40-83,

660 10.1080/10643389.2011.604248, 2013.

661 Kim, J., Kim, T., Lee, Y. E., and Im, S.: Spatial and temporal variability of forest fires in the Republic of

662 Korea over 1991-2020, *Natural Hazards*, 121, 9801-9821, 10.1007/s11069-025-07169-4, 2025.

663 Kirchmeier-Young, M. C., Malinina, E., Barber, Q. E., Perdomo, K. G., Curasi, S. R., Liang, Y. X., Jain,

664 P., Gillett, N. P., Parisien, M. A., Cannon, A. J., Lima, A. R., Arora, V. K., Boulanger, Y., Melton, J.

665 R., Van Vliet, L., and Zhang, X. B.: Human driven climate change increased the likelihood of the

666 2023 record area burned in Canada, *Npj Climate and Atmospheric Science*, 7, 316, ARTN

667 31610.1038/s41612-024-00841-9, 2024.

668 Koren, I., Kaufman, Y. J., Remer, L. A., and Martins, J. V.: Measurement of the effect of Amazon smoke

669 on inhibition of cloud formation, *Science*, 303, 1342-1345, DOI 10.1126/science.1089424, 2004.

670 Kumar, S. and Kumar, A.: Hotspot and trend analysis of forest fires and its relation to climatic factors in

671 the western Himalayas, *Natural Hazards*, 114, 3529-3544, 10.1007/s11069-022-05530-5, 2022.

672 Lapola, D. M., Pinho, P., Barlow, J., Aragao, L. E. O. C., Berenguer, E., Carmenta, R., Liddy, H. M.,

673 Seixas, H., Silva, C. V. J., Silva-Junior, C. H. L., Alencar, A. A. C., Anderson, L. O., Armenteras,

674 D., Brovkin, V., Calders, K., Chambers, J., Chini, L., Costa, M. H., Faria, B. L., Fearnside, P. M.,

675 Ferreira, J., Gatti, L., Gutierrez-Velez, V. H., Han, Z. G., Hibbard, K., Koven, C., Lawrence, P.,

676 Pongratz, J., Portela, B. T. T., Rounsevell, M., Ruane, A. C., Schaldach, R., da Silva, S. S., von

677 Randow, C., and Walker, W. S.: The drivers and impacts of Amazon forest degradation, *Science*,

678 379, 349+, ARTN eabp862210.1126/science.abp8622, 2023.

679 Lau, K. M., Kim, M. K., and Kim, K. M.: Asian summer monsoon anomalies induced by aerosol direct
680 forcing: the role of the Tibetan Plateau, *Climate Dynamics*, 26, 855-864, 10.1007/s00382-006-0114-
681 z, 2006.

682 Li, Y. W., Dykema, J. A., Peterson, D. A., Feng, X., Shen, X. L., June, N. A., Fromm, M. D., McHardy,
683 T. M., Jacquot, J. L., Pittman, J. V., Daube, B. C., Wofsy, S. C., Dean-Day, J., Rapp, A. D., Bowman,
684 K. P., Cziczo, D. J., Mickley, L. J., Pierce, J. R., and Keutsch, F. N.: Enhanced radiative cooling by
685 large aerosol particles from wildfire-driven thunderstorms, *Science Advances*, 11, eadw6526,
686 ARTN eadw652610.1126/sciadv.adw6526, 2025.

687 Lin, J., Shen, X., Xing, L., Che, H., and Holben, B. N.: Analysis of Aerosol Type and Fine- and Coarse-
688 mode Aerosol Direct Radiative Forcing over Regions in East and Southeast Asia Based on
689 AERONET Version 3 Data, *Aerosol and Air Quality Research*, 21, 200503, 10.4209/aaqr.200503,
690 2021.

691 Liu, G. Y., Li, J., Ying, T., Su, H. X., Huang, X., and Yu, Y.: Increasing Fire Weather Potential Over
692 Northeast China Linked to Declining Bering Sea Ice, *Geophysical Research Letters*, 50,
693 e2023GL105931, ARTN e2023GL10593110.1029/2023GL105931, 2023.

694 Luo, N. A., Zhang, Y., Jiang, Y. Z., Zuo, C., Chen, J. Y., Zhao, W. J., Shi, W. Z., and Yan, X.: Unveiling
695 global land fine- and coarse-mode aerosol dynamics from 2005 to 2020 using enhanced satellite-
696 based monthly inversion data, *Environmental Pollution*, 348, 123838, ARTN
697 12383810.1016/j.envpol.2024.123838, 2024.

698 Ma, Q. H., Wei, L. Y., Wang, Y., Zhang, G. J., Zhou, X. L., and Wang, B.: Fire heat affects the impacts
699 of wildfires on air pollution in the United States, *Science*, 389, 1137-1142, 10.1126/science.ads1957,
700 2025.

701 Ma, W., Feng, Z., Cheng, Z., Chen, S., and Wang, F.: Identifying Forest Fire Driving Factors and Related
702 Impacts in China Using Random Forest Algorithm, 10.3390/fl1050507, 2020.

703 Menon, S., Hansen, J., Nazarenko, L., and Luo, Y. F.: Climate effects of black carbon aerosols in China
704 and India, *Science*, 297, 2250-2253, DOI 10.1126/science.1075159, 2002.

705 Ohneiser, K., Ansmann, A., Witthuhn, J., Deneke, H., Chudnovsky, A., Walter, G., and Senf, F.: Self-
706 lofting of wildfire smoke in the troposphere and stratosphere: simulations and space lidar
707 observations, *Atmospheric Chemistry and Physics*, 23, 2901-2925, 10.5194/acp-23-2901-2023,
708 2023.

709 Pan, Y. D., Birdsey, R. A., Fang, J. Y., Houghton, R., Kauppi, P. E., Kurz, W. A., Phillips, O. L., Shvidenko,
710 A., Lewis, S. L., Canadell, J. G., Ciais, P., Jackson, R. B., Pacala, S. W., McGuire, A. D., Piao, S.
711 L., Rautiainen, A., Sitch, S., and Hayes, D.: A Large and Persistent Carbon Sink in the World's
712 Forests, *Science*, 333, 988-993, 10.1126/science.1201609, 2011.

713 Parisien, M. A., Barber, Q. E., Bourbonnais, M. L., Daniels, L. D., Flannigan, M. D., Gray, R. W.,
714 Hoffman, K. M., Jain, P., Stephens, S. L., Taylor, S. W., and Whitman, E.: Abrupt, climate-induced
715 increase in wildfires in British Columbia since the mid-2000s, *Communications Earth &
716 Environment*, 4, ARTN 30910.1038/s43247-023-00977-1, 2023.

717 Parks, S. A., Holsinger, L. M., Panunto, M. H., Jolly, W. M., Dobrowski, S. Z., and Dillon, G. K.: High-
718 severity fire: evaluating its key drivers and mapping its probability across western US forests,
719 *Environmental Research Letters*, 13, 044037, ARTN 04403710.1088/1748-9326/aab791, 2018.

720 Pei, Q., Zhao, C., Yang, Y., Chen, A., Cong, Z., Wan, X., Zhang, H., and Wu, G.: Wildfires heat the

721 middle troposphere over the Himalayas and Tibetan Plateau during the peak of fire season,
722 Atmospheric Chemistry and Physics, 25, 10443-10456, 10.5194/acp-25-10443-2025, 2025.

723 Pinto, M. M., DaCamara, C. C., Hurduc, A., Trigo, R. M., and Trigo, I. F.: Enhancing the fire weather
724 index with atmospheric instability information, Environmental Research Letters, 15, 0940b0947,
725 10.1088/1748-9326/ab9e22, 2020.

726 Qian, Y.: Burning questions on wildfire, Science, 389, 1086-1087, 10.1126/science.aea7430, 2025.

727 Rogeau, M. P. and Armstrong, G. W.: Quantifying the effect of elevation and aspect on fire return
728 intervals in the Canadian Rocky Mountains, Forest Ecology and Management, 384, 248-261,
729 10.1016/j.foreco.2016.10.035, 2017.

730 Santos, L. C., Lima, M. M., Bento, V. A., Nunes, S. A., DaCamara, C. C., Russo, A., Soares, P. M. M.,
731 and Trigo, R. M.: An Evaluation of the Atmospheric Instability Effect on Wildfire Danger Using
732 ERA5 over the Iberian Peninsula, Fire, 6, 120, 2023.

733 Sharples, J. J., Mills, G. A., and McRae, R. H. D.: Extreme drying events in the Australian high-country
734 and their implications for bushfire risk management, Australian Meteorological and Oceanographic
735 Journal, 62, 157-169, 10.22499/2.6203.004, 2012.

736 Su, H. X., Yu, Y., Guo, W. D., and Mao, J. F.: Convective potential and fuel availability complement
737 near-surface weather in regulating global wildfire activity, Science Advances, 11, eadp7765, ARTN
738 eadp776510.1126/sciadv.adp7765, 2025.

739 Tang, W. Y., Llorc, J., Weis, J., Perron, M. M. G., Basart, S., Li, Z. C., Sathyendranath, S., Jackson, T.,
740 Rodriguez, E. S., Proemse, B. C., Bowie, A. R., Schallenberg, C., Strutton, P. G., Matear, R., and
741 Cassar, N.: Widespread phytoplankton blooms triggered by 2019-2020 Australian wildfires, Nature,
742 597, 370+, 10.1038/s41586-021-03805-8, 2021.

743 Tian, X. R., Zhao, F. J., Shu, L. F., and Wang, M. Y.: Distribution characteristics and the influence factors
744 of forest fires in China, Forest Ecology and Management, 310, 460-467,
745 10.1016/j.foreco.2013.08.025, 2013.

746 Van Wagner, C. E.: Development and structure of the Canadian Forest Fire Weather Index System.
747 Canadian Forestry Service, Headquarters, Ottawa, 1987.

748 Veraverbeke, S., Rogers, B. M., Goulden, M. L., Jandt, R. R., Miller, C. E., Wiggins, E. B., and Randerson,
749 J. T.: Lightning as a major driver of recent large fire years in North American boreal forests, Nature
750 Climate Change, 7, 529+, 10.1038/Nclimate3329, 2017.

751 Walker, X. J., Rogers, B. M., Veraverbeke, S., Johnstone, J. F., Baltzer, J. L., Barrett, K., Bourgeau-
752 Chavez, L., Day, N. J., de Groot, W. J., Dieleman, C. M., Goetz, S., Hoy, E., Jenkins, L. K., Kane,
753 E. S., Parisien, M. A., Potter, S., Schuur, E. A. G., Turetsky, M., Whitman, E., and Mack, M. C.:
754 Fuel availability not fire weather controls boreal wildfire severity and carbon emissions, Nature
755 Climate Change, 10, 1130-1136, 10.1038/s41558-020-00920-8, 2020.

756 Wang, B., Spessa, A. C., Feng, P. Y., Hou, X., Yue, C., Luo, J. J., Ciais, P., Waters, C., Cowie, A., Nolan,
757 R. H., Nikonovas, T., Jin, H. D., Walshaw, H., Wei, J. H., Guo, X. W., Liu, D. L., and Yu, Q.: Extreme
758 fire weather is the major driver of severe bushfires in southeast Australia, Science Bulletin, 67, 655-
759 664, 10.1016/j.scib.2021.10.001, 2022a.

760 Wang, H., Jin, B., Zhang, K., Aktar, S., and Song, Z.: Effectiveness in Mitigating Forest Fire Ignition
761 Sources: A Statistical Study Based on Fire Occurrence Data in China, 10.3390/fire5060215,
762 2022b.

763 Wang, W. W., Wang, X. L., Wu, W. L., Guo, F. T., Park, J. N., and Wang, G. Y.: Burn Severity in Canada's

764 Mountain National Parks: Patterns, Drivers, and Predictions, *Geophysical Research Letters*, 49,
765 ARTN e2022GL09794510.1029/2022GL097945, 2022c.

766 Wang, W. W., Wang, X. L., Flannigan, M. D., Guindon, L., Swystun, T., Castellanos-Acuna, D., Wu, W.
767 L., and Wang, G. Y.: Canadian forests are more conducive to high-severity fires in recent decades,
768 *Science*, 387, 91-+, 10.1126/science.ado1006, 2025.

769 Ward, M., Tulloch, A. I. T., Radford, J. Q., Williams, B. A., Reside, A. E., Macdonald, S. L., Mayfield,
770 H. J., Maron, M., Possingham, H. P., Vine, S. J., O'Connor, J. L., Massingham, E. J., Greenville, A.
771 C., Woinarski, J. C. Z., Garnett, S. T., Lintermans, M., Scheele, B., Carwardine, J., Nimmo, D. G.,
772 Lindenmayer, D. B., Kooyman, R. M., Simmonds, J. S., Sonter, L. J., and Watson, J. E. M.: Impact
773 of 2019-2020 mega-fires on Australian fauna habitat, *Nature Ecology & Evolution*, 4, 1321-+,
774 10.1038/s41559-020-1251-1, 2020.

775 Whitman, E., Parisien, M. A., Thompson, D. K., Hall, R. J., Skakun, R. S., and Flannigan, M. D.:
776 Variability and drivers of burn severity in the northwestern Canadian boreal forest, *Ecosphere*, 9,
777 e02128, ARTN e0212810.1002/ecs2.2128, 2018.

778 Xu, C. and You, C.: Climate-linked increasing vegetation fires in global high mountains, *Ecography*,
779 2022, e06527, <https://doi.org/10.1111/ecog.06527>, 2022.

780 Xu, R., Yu, Y., Meng, X. L., Xue, H. W., Zhao, C. F., and Lin, J. T.: Atmospheric Convection and Aerosol
781 Absorption Boost Wildfire Smoke Injection, *Geophysical Research Letters*, 52, e2025GL115989,
782 ARTN e2025GL11598910.1029/2025GL115989, 2025.

783 Yan, X., Zuo, C., Li, Z. Q., Chen, H. W., Jiang, Y. Z., Wang, Q., Wang, G. Q., Jia, K., Yinglan, A., Chen,
784 Z. Y., and Chen, J. Y.: Substantial Underestimation of Fine-Mode Aerosol Loading from Wildfires
785 and Its Radiative Effects in Current Satellite-Based Retrievals over the United States,
786 *Environmental Science & Technology*, 58, 15661-15671, 10.1021/acs.est.4c02498, 2024.

787 Yang, X., Wang, Y., Zhao, C., Fan, H., Yang, Y., Chi, Y., Shen, L., and Yan, X.: Health risk and disease
788 burden attributable to long-term global fine-mode particles, *Chemosphere*, 287, 132435,
789 10.1016/j.chemosphere.2021.132435, 2022.

790 Yang, X. C., Zhao, C. F., Yang, Y. K., and Fan, H.: Long-term multi-source data analysis about the
791 characteristics of aerosol optical properties and types over Australia, *Atmospheric Chemistry and
792 Physics*, 21, 3803-3825, 10.5194/acp-21-3803-2021, 2021a.

793 Yang, X. C., Zhao, C. F., Yang, Y. K., Yan, X., and Fan, H.: Statistical aerosol properties associated with
794 fire events from 2002 to 2019 and a case analysis in 2019 over Australia, *Atmospheric Chemistry
795 and Physics*, 21, 3833-3853, 10.5194/acp-21-3833-2021, 2021b.

796 Yang, X. C., Zhao, C. F., Zhao, W. J., Fan, H., and Yang, Y. K.: Characterization of global fire activity
797 and its spatiotemporal patterns for different land cover types from 2001 to 2020, *Environmental
798 Research*, 227, 115746, ARTN 11574610.1016/j.envres.2023.115746, 2023.

799 Yu, P. F., Toon, O. B., Bardeen, C. G., Zhu, Y. Q., Rosenlof, K. H., Portmann, R. W., Thornberry, T. D.,
800 Gao, R. S., Davis, S. M., Wolf, E. T., de Gouw, J., Peterson, D. A., Fromm, M. D., and Robock, A.:
801 Black carbon lofts wildfire smoke high into the stratosphere to form a persistent plume, *Science*,
802 365, 587-590, 10.1126/science.aax1748, 2019.

803 Yu, Y. and Ginoux, P.: Enhanced dust emission following large wildfires due to vegetation disturbance,
804 *Nature Geoscience*, 15, 878-+, 10.1038/s41561-022-01046-6, 2022.

805 Yu, Y., Mao, J. F., Thornton, P. E., Notaro, M., Wullschleger, S. D., Shi, X. Y., Hoffman, F. M., and Wang,
806 Y. P.: Quantifying the drivers and predictability of seasonal changes in African fire, *Nature*

807 Communications, 11, 10.1038/s41467-020-16692-w, 2020.
808 Zhang, Q., Wang, Y. X. Z., Xiao, Q. Y., Geng, G. N., Davis, S. J., Liu, X. D., Yang, J., Liu, J. J., Huang,
809 W. Y., He, C. P., Luo, B. H., Martin, R. V., Brauer, M., Randerson, J. T., and He, K. B.: Long-range
810 PM pollution and health impacts from the 2023 Canadian wildfires, *Nature*, 645, 672-678,
811 10.1038/s41586-025-09482-1, 2025.
812 Zhao, J., Yue, C., Wang, J., Hantson, S., Wang, X., He, B., Li, G., Wang, L., Zhao, H., and Luyssaert, S.:
813 Forest fire size amplifies postfire land surface warming, *Nature*, 633, 828-834, 10.1038/s41586-
814 024-07918-8, 2024.
815 Zheng, B., Ciais, P., Chevallier, F., Chuvieco, E., Chen, Y., and Yang, H.: Increasing forest fire emissions
816 despite the decline in global burned area, *Science Advances*, 7, eabh2646, ARTN
817 eabh264610.1126/sciadv.abh2646, 2021.
818